Proceedings of IMECE-2000
Control of Vibration and Noise - New Millennium

PRECISION ACTUATION OF MICRO-SPACE STRUCTURES

Shyh-Shiuh Lih [1], Gregory Hickey [1], D.W. Wang [2], and H. S. Tzou [2]

[1] Jet Propulsion Laboratory
California Institute of Technology, Pasadena, CA 91109
[2] Department of Mechanical Engineering, StrucTronics Lab
University of Kentucky, Lexington, KY 40506-0108

ABSTRACT

Space exploration and communication satellites and space structures need deployable precision mirrors, reflectors, and antennas. Conventional deployable space structures require motors and kinematic mechanisms to assist the deployment process. These mechanisms have the potential to jam or tangle and thus jeopardize the entire space mission. Recent development of smart structures and structronic systems opens many new design options in precision structures and systems. This paper reports a study of precision actuation and control for micro-shell laminated space structures made of smart materials. New design concepts of deployable micro-shell laminated structures are discussed and conceptual models fabricated. Analysis of precision parabolic struts is carried out and actuation authorities of proposed configurations are evaluated.

INTRODUCTION

Modern space exploration and communication require large reflectors, solar panels, antennas, and mirrors that are lightweight and deployable. Conventional lightweight deployable space structures often utilize kinematic mechanisms driven by motors in the deployment process (Greschik, 1995). Figure 1 (a&b, courtesy of NASA and NASDA) shows two large deployable antennas: 1) NASA Galileo Space Probe (Space News, 1999) and 2) NASDA Cellular Satellite (NASDA, 1999). Note that deployable Struts that provide structural stability and strength are used in all these three designs.

Recent research and development of smart structures and structronic systems reveal many new design opportunities in sensors, actuators, precision systems, mechatronic systems, and adaptive structures (Tzou and Anderson, 1992; Tzou, 1998). Accordingly, incorporating smart materials to lightweight deployable flexible micro-space structures is a natural trend and this technology needs to be developed quickly. The new design concepts utilize smart materials: piezoelectric materials and shape memory alloys in the design of new "smart" deployable micro-space structures. In these designs shape memory materials are used in the deployment process and piezoelectric materials (bimorphs or laminated structures) are used for precision control and final shape tuning. This paper evaluates the precision control of struts of the micro-space shell structure. Two design concepts showing

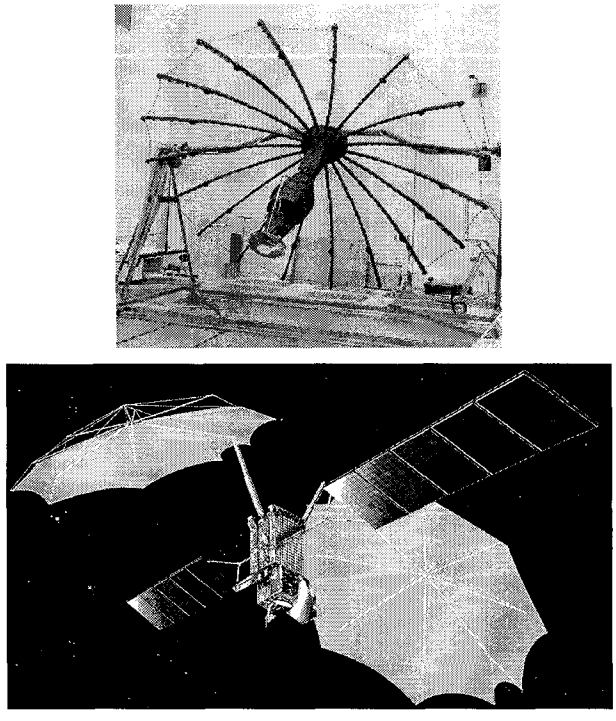

Fig. 1 NASA Galileo Space Probe (Space News, 1999) and NASDA Cellular Satellite (NASDA, 1999)

parabolic shells supported by deployable precision struts are illustrated in Figures 2 and 3. Since piezoelectric laminates are associated with the precision adjustment, accurate modeling and analysis of precision laminates is essential to the successful design of deployable precision lightweight shell structures. The organization of this paper is the modeling and analysis of precision piezoelectric struts will be presented first, followed by detailed analysis of precision piezoelectric bimorph and laminated struts.

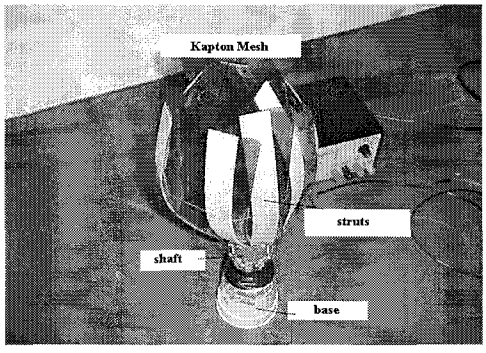

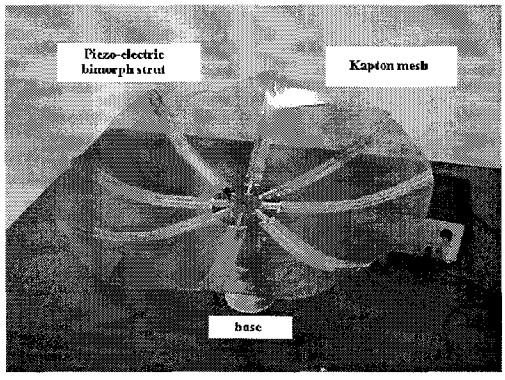

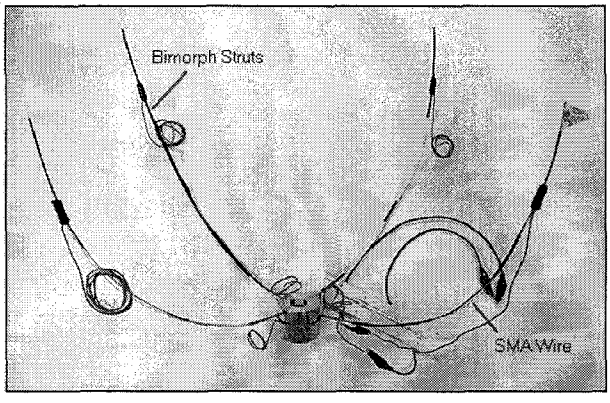

Fig. 3 Conceptual model with SMA and piezoelectric bimorph or laminated struts.

Fig. 2 Stowed and deployed flexible structure.

MODELING OF PARABOLIC PRECISION STRUTS

This study considers two precision piezoelectric parabolic beams: the bimorph parabolic beam and the parabolic laminated beam, which are the constituent elements for the baseline precision micro-space shell structures.

Case 1: Parabolic Bimorph Struts

Piezoelectric bimorph beams have been shown by Tzou for precision microactuation, positioning, indication, and manipulation in high-precision operations (Tzou, 1989). A piezoelectric bimorph strut is made of two piezoelectric layers laminated together with opposite polarity. Parabolic struts have found uses in many practical applications. Figure 4 illustrates the model used for cantilever piezoelectric parabolic bimorph strut (Note that the mesh is used in the finite element modeling and analysis presented later.)

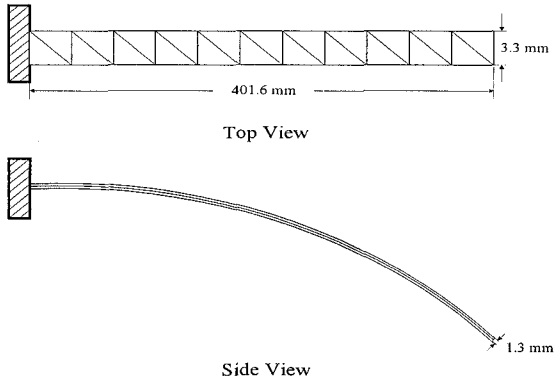

Fig. 4 A curved piezoelectric bimorph strut.

In the development of piezoelectric parabolic bimorph beam, two pieces of piezoelectric materials are bonded together forming a basic bimorph beam structure (Tzou, 1989). It should be noted that the polarized directions of the two layers are opposite to each other in order to introduce a bending effect in the bimorph beam when an external control voltage is applied across the thickness of the parabolic bimorph. Figure 5 illustrates the bending effect due to the voltage induced converse effect.

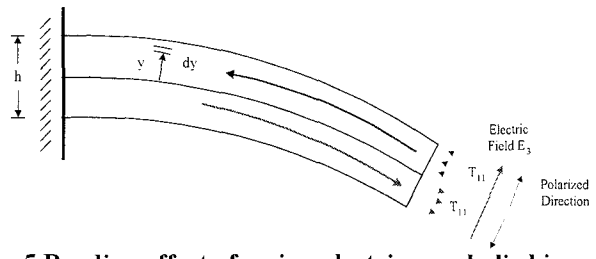

Fig. 5 Bending effect of a piezoelectric parabolic bimorph subjected to external voltage.

The normal stress T_{11} in the upper layer is in compression while the lower layer in tension when a positive voltage E_3 is applied. Stress multiplied by a cross-section area (width b×infinitesimal height dy) gives an equivalent force dF:

$$dF = be_{31}E_3 dy, \tag{1}$$

And this force multiplied a moment arm y yields a bending moment. Thus, the bending moment M with respect to the neutral axis can be calculated as

$$dM = be_{31}E_3 y dy, \tag{2-a}$$

$$M = \int_{-h/2}^{h/2} be_{31}E_3 y dy = e_{31}E_3\left(\frac{bh^2}{4}\right), \tag{2-b}$$

where h is the thickness; b is the width; y is the moment arm; e_{31} is the piezoelectric stress coefficient; and E_3 is strength of electric field and assumed that it is the uniformly distributed over the surface. According to Castigliano's theory on deflection, the angular displacement β of the point of application of the moment M is determined by the equation (Boresi, 1978)

$$\beta = \frac{\partial C}{\partial M}, \tag{3}$$

where the complementary energy C can be expressed as

$$C = \int \frac{M^2 R}{2YI} d\psi, \tag{4}$$

Thus, the angular displacement can by calculated by

$$\beta = \int \frac{MR}{YI} d\psi, \tag{5}$$

where I is the area moment of inertia ($I = bh^3/12$); Y is the Young's modulus; R is the curvature radium and ψ is the central angle; and $E_3 = V/h$ for a uniformly distributed field. If V is only a function of time and independent of space, the equation above can be further written as

$$\beta = \int \frac{e_{31}\left(\frac{V}{h}\right)\left(\frac{bh^2}{4}\right)}{\frac{bh^3}{12}} R d\psi = \frac{3e_{31}VR}{Yh^2}\psi, \tag{6}$$

The above equation provides a relationship between the angular deflection and the applied voltage V of the cantilever bimorph beam. The angular deformation of the free end of the beam, β^*, can be calculated by

$$\beta^* = \frac{3e_{31}VR}{Yh^2}\psi_0 = \frac{3e_{31}L}{Yh^2}V, \tag{7}$$

where ψ_0 is the original central angle and L is the length of the beam. From the geometric relationship shown in Figure 6, one can derive the central angle after deformation, ψ_1,

$$\psi_1 = \psi_0 - \beta^*, \tag{8}$$

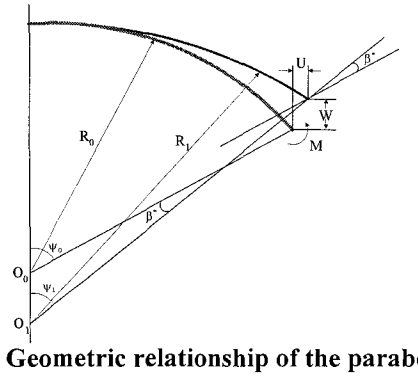

Fig. 6 Geometric relationship of the parabolic bimorph beam.

Then, the transverse, horizontal and the absolute displacements at the free end of the beam are:

$$W = (R_0 - R_1) + (R_1\cos\psi_1 - R_0\cos\psi_0), \tag{9-a}$$

$$U = R_0\sin\psi_0 - R_1\sin\psi_1, \tag{9-b}$$

$$S = \sqrt{W^2 + U^2}, \tag{9-c}$$

where R_0 and R_1 are the original curvature radius and the curvature radius after deformation, respectively; O_0, O_1 are the original center of curvature and the center of curvature after deformation, respectively.

Case 2: Parabolic Laminated Struts

Parabolic beams have a major radius and a minor radius. However, if these radii are equal, parabolic beams

become semicircular beams. For verification purpose, analytical solutions of semicircular beams are calculated in this section. The laminated beam is an elastic beam sandwiched between two layers of piezoelectric materials acting as actuators/sensors respectively. For this analysis polyvinylidene diflouride (PVDF) is used as the piezoelectric material. Since the thickness of the two pieces of the piezoelectric layer is very small (here we ignore the effect of the PVDF's to the static deformation), it is convenient to use polar coordinates.

For a cross section of the semicircular beam located at angle θ from the section on which a concentrated force P is applied at the tip end as shown in Figure 7, we have

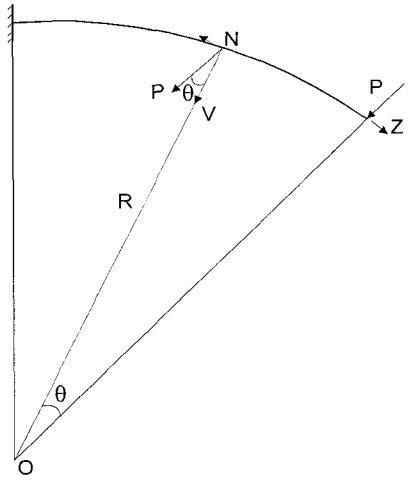

Fig. 7 A semicircular beam subjected to the concentrated force.

$$N = P\sin\theta,\ \frac{\partial N}{\partial P} = \sin\theta;\ V = P\cos\theta,\ \frac{\partial V}{\partial P} = \cos\theta,\ \text{(10-a,b)}$$

$$M = PR\sin\theta,\ \frac{\partial M}{\partial P} = R\sin\theta, \qquad \text{(10-c)}$$

where N, V and M are the normal force, shear force and moment which is generated by P at angle θ. According to Castigliano's theory on deflection, the displacement w in the direction of which force P is applied is determined by the equation

$$w = \frac{\partial U}{\partial P} = \int \frac{N}{EA}\frac{\partial N}{\partial P}dz + \int \frac{kV}{GA}\frac{\partial V}{\partial P}dz + \int \frac{M}{EI}\frac{\partial M}{\partial P}dz, \qquad (11)$$

The equation above can be further written as:

$$w = \int_0^\theta \frac{P\sin\theta}{EA}\sin\theta R d\theta + \int_0^\theta \frac{1.5P\cos\theta}{GA}\cos\theta d\theta + \int_0^\theta \frac{PR\sin}{EI} R\sin\theta R d\theta, \qquad (12)$$

Vibration control of the laminated struts is discussed next.

For a parabolic beam strut, the curvilinear coordinates α_1 and α_2 are specified by ϕ and x respectively. The Lamé parameters A_i and radii of curvatures R_i are respectively defined by $A_1 = \frac{b}{\cos^3\phi}, A_2 = 1,$ $R_1 = \frac{b}{\cos^3\phi}, R_2 = \infty$ where b is constant. The closed-form control equations are

$$-\frac{\partial \tilde{N}_{11}}{\partial\phi} - \frac{\partial(\tilde{N}_{21}A_1)}{\partial x} - \frac{1}{R_1}\left[\frac{\partial \tilde{M}_{11}}{\partial\phi} + \frac{\partial(\tilde{M}_{21}A_1)}{\partial x}\right] + A_1\rho h\ddot{u}_1 = A_1F_1 \qquad (13)$$

$$-\frac{\partial}{\partial\phi}\left\{\frac{1}{A_1}\left[\frac{\partial \tilde{M}_{11}}{\partial\phi} + \frac{\partial(\tilde{M}_{21}A_1)}{\partial x}\right]\right\} - \frac{\partial}{\partial x}\left\{\frac{\partial \tilde{M}_{12}}{\partial\phi} + \frac{\partial(\tilde{M}_{22}A_1)}{\partial x}\right\} + A_1\frac{\tilde{N}_{11}}{R_1} + A_1\rho h\ddot{u}_3 = A_1F_3 \qquad (14)$$

where the ~ terms include the elastic component and the feedback control component induced by the converse piezoelectric effect, e.g., $\tilde{N}_{11} = N_{11} + \tilde{N}^a_{11}$, $\tilde{M}_{11} = M_{11} + \tilde{M}^a_{11}$ where N_{11} and M_{11} are the elastic components . The in-plane effective forces $\tilde{N}^a_{ii}$ and moment $\tilde{M}^a_{ii}$ induced by the imposed actuator voltage ϕ^a can be expressed as (Tzou, 1993)

$$\tilde{N}^a_{11} = d_{31}Y_p\phi^a\ ;\ \tilde{N}^a_{22} = d_{32}Y_p\phi^a \qquad (15)$$

$$\tilde{M}^a_{11} = r^a_1 d_{31}Y_p\phi^a\ ;\ \tilde{M}^a_{22} = r^a_2 d_{31}Y_p\phi^a \qquad (16)$$

where Y_p is Young's modulus of the piezoelectric actuator; r^a_i is the effective moment arm; A_i is Lamé parameter; R_i is curvature radius. Note that the control algorithms determine the imposed actuator voltage ϕ^a. For the velocity feedback, the sensor signal ϕ^s used in control components is replaced by $\dot{\phi}^s$, i.e.,

$\dot{\phi}^s = \frac{\partial}{\partial t}\left[\phi^s(u_1, u_2, u_3, t)\right] = \phi^s(\dot{u}_1, \dot{u}_2, \dot{u}_3, t)$, and usually amplified by the gain factor G.

$$\tilde{N}^a_{11} = -G \cdot d_{31} Y_p \dot{\phi}^s; \quad \tilde{N}^a_{22} = -G \cdot d_{32} Y_p \dot{\phi}^s \tag{17}$$

$$\tilde{M}^a_{11} = -G \cdot r_1^a d_{31} Y_p \dot{\phi}^s; \quad \tilde{M}^a_{22} = -G \cdot r_2^a d_{32} Y_p \dot{\phi}^s \tag{18}$$

For independent modal control, the parabolic beam equations are transferred to the modal domain

$u_i(\theta, t) = \sum_{k=1}^{\infty} \eta_k(t) U_{3k}(\theta)$ and, thus, modal control effects can be evaluated independently. Studies of prototype models are evaluated next.

CASE STUDIES

Scaled mockup models of the micro-space structures were presented in Figures 2 and 3. Piezoelectric bimorphs or piezoelectric laminates were used as the parabolic structural struts for precision control of the final micro-shell structures. These two configurations are analyzed as case studies and theoretical solutions are compared with numerical results.

Case 1: Parabolic Bimorph Struts

For this case a parabolic piezoelectric bimorph strut is made of two piezoelectric (PVDF) layers laminated together with opposite polarity. The beam is 401.6 mm long, 3.3 mm wide and 2×0.65 mm thick. All geometric and material properties are provided in Table 1. The beam is modeled as an assemblage of 280 identical triangular elements, 140 for each layer and 70 meshes along the beam length (Tzou and Ye, 1996; Hom and Shankar, 1996). The left end is clamped and the right is free (see Figure 4). A unit voltage (1 V) is applied across the thickness. The objective of this model is to evaluate the precision actuation capability and to verify the converse piezoelectric effect by applying a constant voltage on the parabolic bimorph struts. Two fundamental techniques, namely, theoretical and finite element methods, are used in the analysis of the parabolic piezoelectric bimorph beam struts of the micro-space structures. Table 2 summarizes the theoretical and finite element results of the constant-radius beam struts with various angles (0-90°) and compares the analytical solutions and numerical result.

Table 1: Geometric and material properties.

Length, L (m)	0.4016
Width, b (m)	3.3×10^{-3}
Thickness, h (m)	0.5×10^{-4}
Density, ρ (Kgm^{-3})	1.8×10^{3}
Young's modulus, Y (Pa)	2.0×10^{9}
Poisson's constant, μ	0.29
Piezostrain constant, d_{31} (mV^{-1})	0.22×10^{-10}
Electric permitivity, ε_{11} (Fm^{-1})	1.062×10^{-10}

Table 2: Comparisons of theoretical and finite element results of parabolic beam struts.

Angle (deg)		0	1	15	30	45	60	75	90
Theory	W	3.2931	3.2922	3.2362	3.0702	2.8018	2.4433	2.0107	1.5233
Disp. (m)×10^{-6}	U	1.8×10^{-5}	0.0383	0.5707	1.1181	1.6199	2.0561	2.4100	2.6687
(Free end)	S	3.2931	3.2924	3.2862	3.2674	3.2364	3.1933	3.1387	3.0729
FEM	W	3.1493	3.1494	3.1338	3.0832	2.9981	2.8813	2.7357	2.5653
Disp. (m)×10^{-6}	U	0.0102	0.0285	0.2843	0.5533	0.8116	1.0542	1.2765	1.4745
(Free end)	S	3.1493	3.1496	3.1467	3.1325	3.1060	3.0682	3.0189	2.9589

Angle (deg)		0	1	15	30	45	60	75	90
Theory Disp. (m)×10^{-6} (Free end)	S	3.2931	3.2924	3.2862	3.2674	3.2364	3.1933	3.1387	3.0729
FEM Disp. (m)×10^{-6} (Free end)	S	3.1493	3.1496	3.1467	3.1325	3.1060	3.0682	3.0189	2.9589
Error (%)		4.36	4.33	4.24	4.13	4.03	3.91	3.82	3.71

The static deformation of the free end of the parabolic bimorph beam struts has two deformation components: the transverse deformation and the horizontal deformation. It is observed that the transverse displacement component increases and the horizontal displacement component decreases with the increment of central angle. And the total static deformation decreases with the increment of the central angle. The analytical and numerical results are compared very well and the error range is within 5%. Also, the precision actuation capability is excellent and suitable in micro-shell actuation and control.

Case 2: Laminated Parabolic Struts

The parabolic beam studied here is laminated with two pieces of PVDFs on the top and bottom surfaces of a flexible beam strut. It has parabolic curvature radius in the longitudinal direction, and infinite curvature radius in the width direction as shown in Figure 8 (beam B). (Note that beams A and C are constant radius beam, in which the minor radius is the radius of beam A and the major radius is the radius of beam C.) It is assumed that the inner piezoelectric layer serves as a distributed sensor, the outer layer serves as a distributed actuator. All geometric and material properties are provided in Table 3.

The beam is clamped at the left end and the right end is free. A point force with magnitude of 0.01 N is applied at the tip end. In FE analysis, the beam strut is modeled with 300 triangular shell elements, 100 for each layer, and 50 meshes along the strut length.

Table 3 Geometric and material properties.

Properties	PVDF	Steel
Length, L (m)	0.4016	0.4016
Width, b (m)	3.3×10^{-3}	3.3×10^{-3}
Thickness, h (m)	0.5×10^{-4}	1.3×10^{-3}
Density, ρ (Kgm^{-3})	1.8×10^{3}	7.8×10^{3}
Young's modulus, Y (Pa)	2.0×10^{9}	2.1×10^{11}
Poission's constant, μ	0.29	0.30
Piezostrain constant, d_{31} (mV^{-1})	0.22×10^{-10}	
Electric permittivity, ε_{11} (Fm^{-1})	1.062×10^{-10}	

Case 2.1 Static Actuation

The minimum and maximum curvature radii of the parabolic beam B are 0.52686 m and 0.9679 m, respectively. Two additional constant-radius beam struts (A and C), i.e., beam A has a constant curvature radius 0.52686m and beam C has a constant curvature radius 0.9679m, are studied. Based on the analytical derivations presented previously, the transverse static deformation (W) of the tip end of the parabolic beam B should be smaller than that of beam A and larger than that of beam C, and the horizontal static deformation (U) should be larger than that of beam A and smaller than that of beam C. The static deformations of the tip end of these three ring shells are provided in Table 4; comparisons are outlined in Table 5.

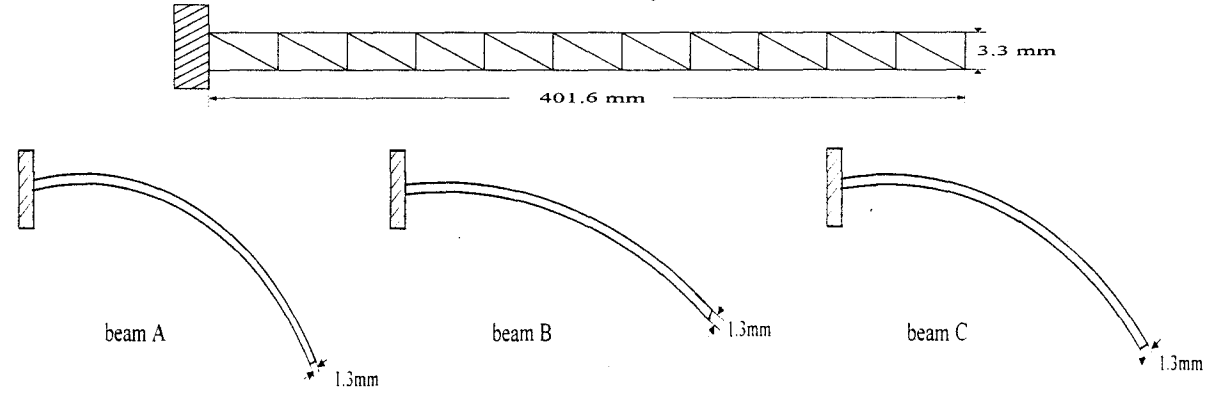

Fig. 8 Circular struts (A & C) and parabolic strut (B).

Table 4: Static deformations of the tip end of the beams.

	Beam A	Beam B	Beam C
W	0.151349D-02	0.160175D-02	0.164002D-02
U	0.444910D-03	0.321288D-03	0.260831D-03
S	0.1577528D-2	0.1633655D-2	0.1660632D-2

Case 2.2 Dynamic Analysis and Control

In dynamic analysis, an initial displacement is imposed at the free end. The initial damping ratio is assumed to be 0.2% and the total time with a time step $\Delta t = 2.5\times10^{-3}$ second is set to be 5 seconds. The first natural frequency is 6.7488 Hz; the free displacement response of the tip end is shown in Figure 9. Controlled responses under the negative velocity control are shown in Figures 10-14, and the inferred damping ratios at different gains are plotted in Figure 15.

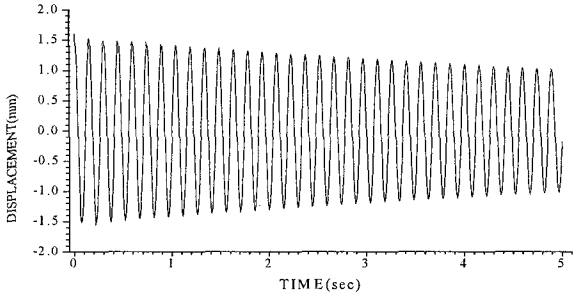

Fig. 9 Free displacement response of the tip end.

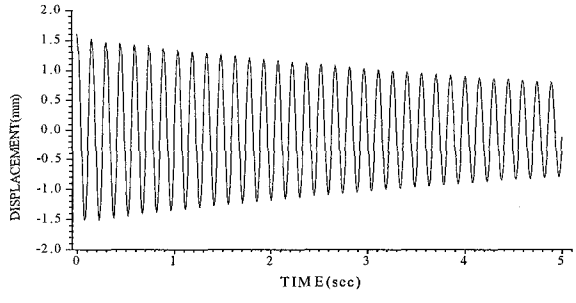

Fig. 10 Controlled response of the tip end (gain=0.2).

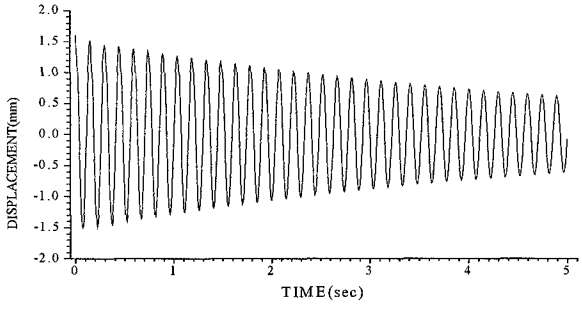

Fig. 11 Controlled response of the tip end (gain=0.4).

Table 5: Transverse deformations of tip end of beams.

	Beam A	Beam C
Analytical solution	1.5146×10^{-3}	1.6437×10^{-3}
Numerical solution	0.151349D-02	0.164002D-02
Percentage error	0.073	0.22

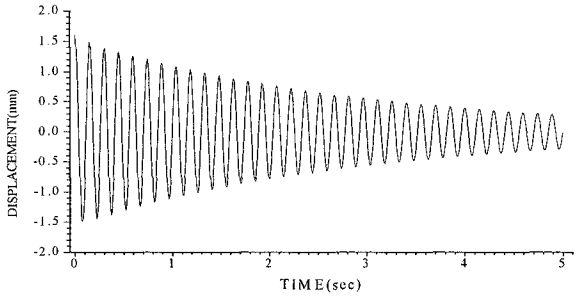

Fig. 12 Controlled response of the tip end (gain=1.0).

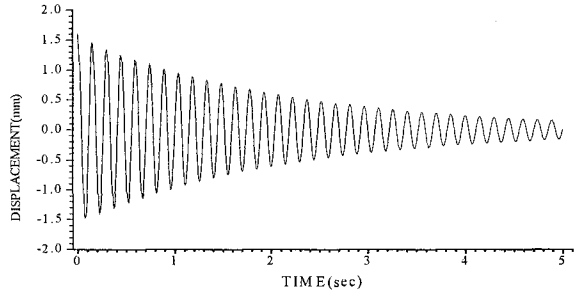

Fig. 13 Controlled response of the tip end (gain=1.5).

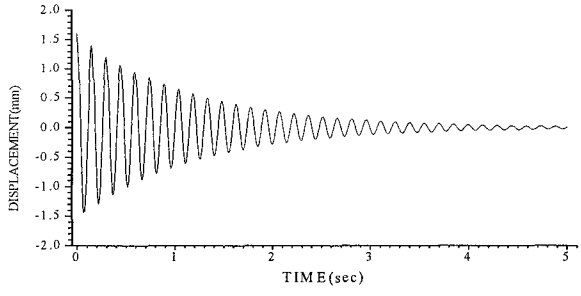

Fig. 14 Controlled response of the tip end (gain=3.0).

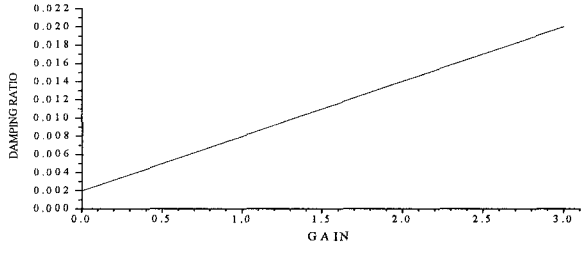

Fig. 15 Inferred damping ratios with different gains.

CONCLUSIONS

Space exploration and communication require deployable precision deployable structures: mirrors, reflectors, and antennas. Conventional deployable space structures use motors and kinematic mechanisms to assist the deployment process, which would jeopardize the whole mission if jammed or tangled. Recent development of smart structures and structronic systems open much new design options in precision deployable structures and systems. Precision actuation and control of micro-shell space structures made of smart materials such as those evaluated in this paper enable a new class of space mechanisms. The mathematical and finite element models of the baseline parabolic actuation struts demonstrate the feasibility of these designs. The actuation and control capabilities of laminated parabolic struts were analyzed and the analytical solutions show very good agreement and correlation with finite element results. This study demonstrates the feasibility of precision actuation and control capabilities of deployable shell-type micro-space structures.

ACKNOWLEDGEMENT

This research is supported by the Deformable Thin Shell Nano-Laminate Mirror Task at Jet Propulsion Laboratory, California Institute of Technology under contract with the National Aeronautics and Space Administration. Contributing to this work were helped by Yasser Al-Saffar, Andrew Clem, Ron Couch, Jim Jackson, Craig Moseley, Chris Kuhn, Jason Clark, Kathy Hardesty, and Casey McIntosh in the Department of Mechanical Engineering at the University of Kentucky.

REFERENCES

Boresi, P., 1978, "*Advanced Mechanics of Materials*", 3rd ed., John Wiley and Sons, New York.

Greschik, G., 1995, "The Unfolding Deployment of a Shell Parabolic Reflector," 36th SDM Conference, New Orlean, LA, AIAA paper, AIAA-95-1278-Cp.

Hom, C.L. and Shankar, N., 1996, "A finite element method for electrostrictive ceramic devices", *Int. J. Solids & Structures*, Vol. 33, pp.1757-1779.

David, Leonard. Space News, Army Times Publishing Co., 1999.

NASDA, 1999. Internet World Wide Web, http://www.nasda.go.jp/index_e.html .

Tzou, H.S., 1989, "Development of a Light-weight Robot End-effector using Polymeric Piezoelectric Bimorph", *Proceeding of the 1989 IEEE international Conference on Robotics and Automation*, pp.1704-1709.

Tzou, H.S., 1993, *Piezoelectric Shells (Distributed Sensing and Control of Continua)*, Kluwer Academic Publishers, Dordrecht/Boston/London.

Tzou, H.S., 1998, "Multi-field Transducers, Devices, Mechatronic Systems and Structronic Systems with Smart Materials," *Shock and Vibration Digest*, Vol.30, No.4, pp.282-294.

Tzou, H.S. and Anderson, G.L. (Editors), 1982, *Intelligent Structural Systems*, Kluwer Academic Publishers, Dordrecht/Boston/London.

Tzou, H.S. and Ye, R., 1996, "Analysis of Piezoelastic Structures with Laminated Piezoelectric Triangle Shell Element", *AIAA Journal*, Vol. 34, No. 1, pp.110-115.
(PreMicro4.ShpCtrl.Doc600)